J Fluoresc (2011) 21:65–80
DOI 10.1007/s10895-010-0690-5

ORIGINAL PAPER

Synthesis and Photophysics of Some Novel Imidazole Derivatives Used as Sensitive Fluorescent Chemisensors

Kanagarathinam Saravanan · Natesan Srinivasan · Venugopal Thanikachalam · Jayaraman Jayabharathi

Received: 19 February 2010 / Accepted: 21 June 2010 / Published online: 10 July 2010

Abstract Some novel imidazole derivatives were developed for highly sensitive chemisensors for transition metal ions. Since these compounds are sensitive to different external stimulations such as UV irradiation, heat, increasing pressure and changing the environmental pH causing colour change and so they can be used as a ′multi-way′ optically switchable material. A prominent fluorescence enhancement was found in the presence of transition metal ions such as Hg^{2+}, Pb^{2+} and Cu^{2+} and this was suggested to result from the suppression of radiationless transitions from the n-π* state in the chemisensors. The existence of C-H….O intramolecular hydrogen bonding in dmphnpi is confirmed by the Natural Bond Orbital analysis (NBO). The Mulliken, NBO charge analysis and the HOMO-LUMO energies were also calculated. The electric dipole moment (μ) and the first-hyperpolarisability (β) value of the investigated molecules have been studied both experimentally and theoretically which reveal that the synthesized molecules have microscopic non-linear optical (NLO) behaviour with non-zero values. Ground and excited state DFT calculation were carried out in order to find out dipole moment and energy.

Keywords NMR · Emission kinetics · Chemisensors · NLO · HOMO-LUMO

K. Saravanan · N. Srinivasan · V. Thanikachalam · J. Jayabharathi (✉)
Department of Chemistry, Annamalai University, Annamalainagar 608 002 Tamilnadu, India
e-mail: jtchalam2005@yahoo.co.in

Introduction

Recently, heterocyclic imidazole derivatives have attracted considerable attention because of their unique optical properties [1–3]. These compounds play very important role in chemistry as mediators for synthetic reactions, primarily for preparing functionalized materials [4–9]. Imidazole nucleus forms the main structure of some well-known components of human organisms, i.e., the amino acid histidine, vitamin B_{12}, a component of DNA base structure, purines, histamine and biotin and present in structure of many natural or synthetic drug molecules, i.e., azomycin, cimetidine and metronidazole and also have significant analytical applications utilizing their fluorescence and chemiluminescence properties [10–12].

Some basic processes, such as excited state intermolecular proton transfer (ESIPT) have been carried out for imidazole derivatives [13–15]. An important property that makes imidazole derivatives more attractive as a chelator is the appreciable change in its fluorescence upon metal binding. Therefore, imidazole derivatives have been used to construct highly sensitive fluorescent chemisensors for sensing and imaging of metal ions and its chelates in particular those with Ir^{3+} are major components for organic light emitting diodes [2, 3] and are promising candidates for fluorescent chemisensors for metal ions. In the present paper we summarized a comprehensive study of the imidazole derivatives and their structures were characterized by NMR spectra. Photophysical and photochemical studies of imidazole derivatives and their chelates were analysed and discussed. Theoretical calculations were carried out by using Gaussian-03 progam [16, 17] to supplement the experimental results.

Experimental

Materials and methods

1,2-dione (Sigma-Aldrich Ltd.), substituted benzaldehydes (S.D. fine.) and all the other reagents used without further purification.

Optical measurements and composition analysis

NMR spectra were recorded for **1–4** on a Bruker 400 MHz. The ultraviolet–visible (UV–Vis) spectra were measured on UV–Vis spectrophotometer (Perkin Elmer, Lambda 35) and corrected for background due to solvent absorption. Photoluminescence (PL) spectra were recorded on a (Perkin Elmer LS55) fluorescence spectrometer. MS spectra were recorded on a Varian Saturn 2,200 GCMS spectrometer.

Non-linear optical measurements

The non-linear optical conversion efficiencies were parted using a modified set up of Kurtz and Perry. A Q-switched Nd:YAG laser beam of wavelength of 1,064 nm was used with an input power of 4.1 mJ/pulse width of 10 ns, scattering geometry 90°, the repetition rate being 10 Hz, monochromater Jobin Youon Triax 550, slit width 0.5 mm, focal length of focussing lense 20 cm, PMT model number XP2262B used in Philips photonics, power supply for PMT is 1.81 KU/mA with oscilloscope Jektronix TDS 3052B.

Computational details

Quantum mechanical calculations were used to carry out the optimized geometry, NLO, NBO, HOMO-LUMO analysis and TD-DFT with Guassian-03 program using the Becke3-Lee-Yang-Parr (B3LYP) functional supplemented with the standard 6-31G(d,p) basis set [16, 17]. As the first step of our DFT calculation for NLO analysis, the geometry taken from the starting structures were optimized and then, the electric dipole moment μ and β tensor components of the studied compounds were calculated by using B3LYP method at the 6-31G (d, p) basis set level, which has been found to be more than adequate for obtaining reliable trends in the first hyperpolarizability values.

We report the β_{tot} (total first hyperpolarizability) for the investigated molecules **1−4** and the components of the first hyperpolarizability can be calculated using Eq. 1:

$$\beta_i = \beta_{iii} + 1/3 \sum_{i \neq j} (\beta_{ijj} + \beta_{jij} + \beta_{jji}) \quad (1)$$

Using the x, y and z components, the magnitude of the first hyperpolarizability tensor can be calculated by

$$\beta_{tot} = \left(\beta_x^2 + \beta_y^2 + \beta_z^2\right)^{1/2} \quad (2)$$

The complete equation for calculating the magnitude of first hyperpolarizability from Gaussian-03 output is given as follows:

$$\beta_{tot} = \left[\begin{array}{l} (\beta_{xxx} + \beta_{xyy} + \beta_{xzz})^2 + (\beta_{yyy} + \beta_{yzz} + \beta_{yxx})^2 \\ + (\beta_{zzz} + \beta_{zxx} + \beta_{zyy})^2 \end{array} \right]^{1/2} \quad (3)$$

All the electric dipole moment and the first hyperpolarizabilities are calculated by taking the Cartesian coordinate system (x, y, z)=(0, 0, 0) at own center of mass of the compound.

General procedure for the synthesis of imidazole derivatives (**1**–**4**)

The experimental procedure was used as the same as described in our recent paper [18]. The various substituted imidazole derivatives were synthesized from an unusual four components assembling of 1,2-dione, ammonium acetate, arylamine and an arylaldehyde.

4,5-Dimethyl-2-phenyl-1H-imidazole (dpi) , (**1**)

Yield: 50%. mp 96°C, Anal. calcd. for $C_{11}H_{12}N_2$: C, 76.71; H, 7.02; N, 16.27. Found: C, 75.25; H, 6.08; N, 17.08. ^{1}H NMR (400 MHz, $CDCl_3$): δ 7.80 (d, J=8.0 Hz, 2H), 7.30 (t, J=8.0 Hz, 2H), 7.25 (t, J=7.6 Hz, 1H), 3.5 (bs, 1H), 2.12 (s, 6H). ^{13}C (100 MHz, $CDCl_3$): δ 10.5, 130.6, 126.0, 129.9, 132.7. MS: m/z 172.09, calcd 172.10.

4,5-Dimethyl-1,2-diphenyl-1H-imidazole (ddi), (**2**)

Yield: 48%. mp 102°C, Anal. calcd. for $C_{17}H_{16}N_2$: C, 82.21; H, 6.45; N, 11.28. Found: C, 82.07; H, 6.32; N, 11.04. ^{1}H NMR (400 MHz, $CDCl_3$): δ 2.07 (s, 3H), 2.35 (s, 3H), 7.22 (m, 5H), 7.37 (m, 2H), 7.48 (m, 3H). ^{13}C NMR (100 MHz, $CDCl_3$): δ 9.50, 12.58, 71.50, 114.2, 117.3, 128.20, 129.58, 144.35. MS: m/z 248.03, calcd. 248.13.

4,5-Dimethyl-1-phenyl-2-(p-fluorophenyl)-1H-imidazole (dmpfpi), (**3**)

Yield: 40%. mp 125°C, Anal. calcd. for $C_{17}H_{15}FN_2$: C, 76.67; H, 5.68; N, 10.52. Found: C, 75.01; H, 5.36; N, 8.98. ^{1}H NMR (400 MHz, $CDCl_3$): δ 1.99 (s, 3H), 3.85 (s, 3H), 6.85-7.35 (aromatic protons). ^{13}C (100 MHz,

$CDCl_3$): δ 7.0, 12.5, 110.0, 116.5, 122.0 129.1, 135.2, 145.0, 170.0. MS: m/z 266.12, calcd. 266.0.

4,5-Dimethyl-1-phenyl-2-(2′-hydroxy-5′-nitrophenyl) -1H-imidazole (dmphnpi), (**4**)

Yield: 50%. mp 145°C, Anal. calcd. for $C_{17}H_{15}N_3O_3$: C, 66.01; H, 4.85; N, 13.59. Found: C, 65.89; H, 4.76; N, 12.83. ^{1}H NMR (400 MHz, $CDCl_3$): δ 2.14 (s, 6H), 5.8 (m, 5H), 7.23 (s, 1H), 7.0 (d, J=7.5 Hz, 1H), 6.8 (d, J=7.0 Hz, 1H), 9.23(s,1H). ^{13}C (100 MHz, $CDCl_3$): δ 11.0, 131.7, 147.0, 118.0, 127.9, 155.9, 121.9, 115.4, 130.2. MS: m/z 309.0, calcd. 309.08.

Results and discussion

Photophysical properties of imidazole derivatives **1–4** in solution

Absorption and emission properties of imidazole derivatives **1–4** have been studied in various solvents. The absorption band maxima λ_{max}, emission band maxima λ_{max} (em) and the associated Stokes shift (ΔE) together with the fluorescence quantum yields (Φ_f) are shown in Table 1.

It is evident from Fig. 1a–c that λ_{abs} changes slightly when pH of the solution increases but the emission bands are red shifted in acidic acetonitrile solution (pH 2) and blue shifted in the case of very basic acetonitrile solution (pH 11). The red shift of the maximum emission in acid medium and blue shift of maximum emission in basic medium may be due to the presence of increased resonance interaction of the π-cloud of the phenyl ring attached to the carbon of the imidazole ring and the lone pair of nitrogen (N4) of the imidazole ring [19] (Fig. 2). The resonance interaction increases if the lone pair of electrons and the π-cloud is parallel to each other and in order to understand the coplanarity, optimization of imidazole derivatives **1–4,** have been performed by DFT at B3LYP/6-31G(d,p) using Gaussian-03 (Table 2) which also strongly supports the existence of increased resonance interaction of the π-cloud of the phenyl ring attached to the carbon of the imidazole ring and the lone pair of nitrogen of the imidazole ring. From the optimized structures it was found that there is poor coplanarity between the phenyl ring attached to the nitrogen and carbon of the the imidazole ring (**2** and **3)**. The imidazole ring is essentially planar and the angle of tilting of the phenyl ring attachéd to the carbon of the imidazole ring is C5-N4-C8-C9 (-26.68 (**1**), -27.59 (**2**), -25.25 (**3**) and -28.23 (**4**)) and the phenyl ring attached to the nitrogen of the imidazole ring is tilted from the plane of the imidazole ring by an angle of C5-N4-C24-C25 (-69.68º (**2**), -65.59º (**3**) and -62.65º(**4**)). However the angle of tilting is higher in magnitude in the case of phenyl ring attached the nitrogen and the bond lengths of them lie between a C-C single bond (about 1.54 Å) and a C = C double bond (about 1.33 Å) and are close to each other. In very basic acetonitrile solution, the imidazole derivatives ddi (**2**) and dmpfpi (**3**)

Table 1 Photophysical data of imidazole derivatives **1–4**

Solvent	λ_{max} (nm)	λ_f (nm)	Stokes shift	λ_{max} (nm)	λ_f (nm)	Stokes shift	λ_{max} (nm)	λ_f (nm)	Stokes shift	λ_{max} (nm)	λ_f (nm)	Stokes shift
Hexane	282.0	361.5	7798.5	284.3	314.0	3327.0	281.5	385.0	9552.5	284.5	Non-fluorescent	
				284.3								
Benzene	288.0	368.8	7607.3	288.2	368.0	7524.2	284.6	331.0	4931.7	240.1		
										286.5		
Chloroform	285.3	363.0	7502.6	245.0	381.6	9005.8	240.0	377.1	8794.9	285.3		
				284.0			283.2					
Ethyl acetate	284.2	360.0	7408.7	227.0	360.7	7216.7	283.0	367.4	8117.4	284.5		
				286.2								
Dichloro methane	229.0	384.0	8765.2	285.0	380.5	8806.5	229.0	381.5	9079.6	229.0		
	287.3						283.3			286.2		
n-butanol	229.0	368.0	7988.5	226.2	360.0	7628.0	223.5	378.6	9253.1	283.2		
	282.1			282.4			280.4					
Ethanol	226.5	364.0	21389.0	232.7	362.3	7571.9	212.2	364.0	8563.5	209.6		
	283.3			284.3			277.5			282.1		
Methanol	227.0	362.0	7786.5	226.2	361.2	7604.6	210.0	363.0	8511.7	285.1		
	282.4			238.4			277.3					
Acetonitrile	287.5	383.2	8686.6	289.0	363.0	7053.9	239.0	355.0	8819.3	231.5		
							282.1	(sh) 375.6		283.75		

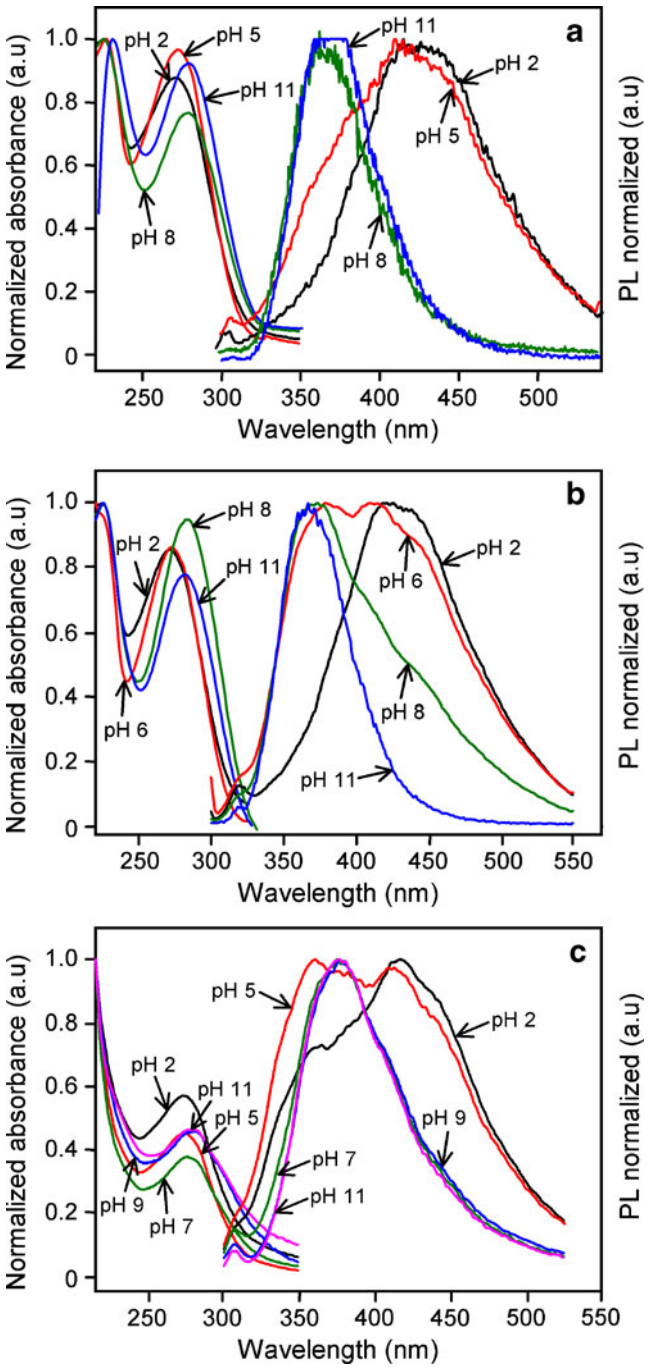

Fig. 1 Normalised absorbance and emission spectra of **1**–**4** at various pH solutions

almost inhibits fluorescence. In the case of dmphnpi **4**, two clear isobestic points observed at 325 and 372 nm (Fig. 3), suggest the presence of two possible species (**4a** and **4b**, Scheme 1) and these observations show that compound dmphnpi **4** undergo deprotonation in basic pH [20].

Solvent effects on the absorption and fluorescence properties

All these imidazole derivatives **1–3** show solvatochromism (Table 1) i.e., changes in the polarity of the solvents, charge transfer takes place and causing colour changes. The position of the longer-wavelength absorption and emission bands in the spectra was determined in several protic and aprotic solvents (Fig. 4a–c). Lippert-Mataga [21] plot was constructed for the normal fluorescence spectrum of imidazole derivatives (**1–3**) (Fig. 5a) using the following equation.

$$\bar{\nu}_{ss} = \bar{\nu}_{ab} - \bar{\nu}_{fl} = const + \left[\frac{2(\mu_e - \mu_g)^2}{hca^3}\right] f(D,n) \qquad (4)$$

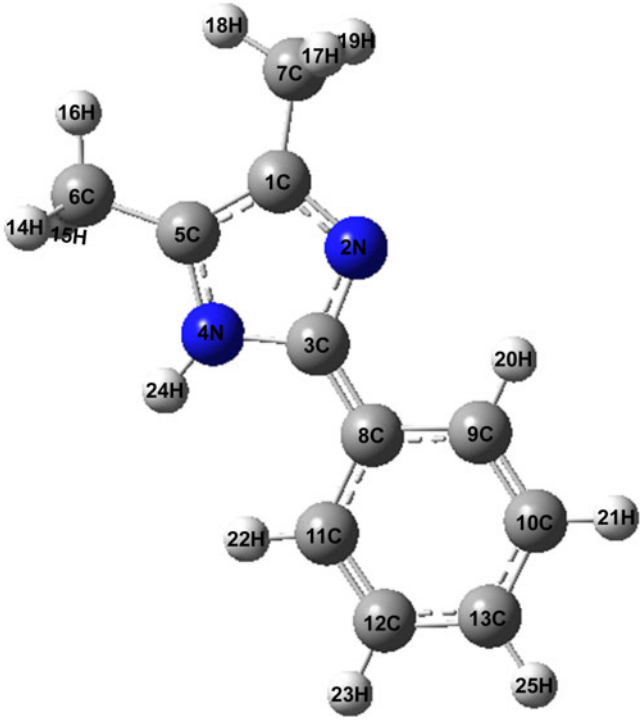

Fig. 2 Excited state optimized structure of dpi **1**

where $f(D,n) = (D-1)/(2D+1) - (n^2-1)/(2n^2+1)$, indicates the orientation polarizability and depicts polarity parameter of the solvent [22], n is refractive index, D is dielectric constant, μ_e and μ_g are dipole moments of the species in S_1 and S_0 states, respectively, h, Planck's constant; c, velocity of light and a, Onsagar's cavity radius. Stokes shifts were calculated from λ^f_{max} rather than 0-0-emission transition. The Lippert-Mataga plot is linear for the non-polar and polar / aprotic solvents with excellent correlation coefficient.

Large Stokes shifted fluorescence band suggest that this emission has originated from the species which is not present in the S_0 state and large geometrical changes have takes place in the species when excited to S_1 state and the large Stokes shift may be explained by the presence of intermolecular hydrogen bonding of imidazole nitrogen (N2) with polar solvent molecules leading to the stabilization of solvated isomers of **1–3** (Fig. 5b).

Quantum yield and photochemical properties of imidazole derivatives **1–3**

The fluorescence quantum yield for compounds **1–3** (Table 3) were measured in acetonitrile, using coumarin 47 in ethanol as a standard according to the equation,

$$\Phi_{unk} = \Phi_{std}\left(\frac{I_{unk}}{I_{std}}\right)\left(\frac{A_{std}}{A_{unk}}\right)\left(\frac{\eta_{unk}}{\eta_{std}}\right)^2 \quad (5)$$

where Φ_{unk}, Φ_{std}, I_{unk}, I_{std}, A_{unk}, Φ_{unk} and Φ_{std} are the fluorescent quantum yields, the integration of the emission intensities, the absorbances at the excitation wavelength

Table 2 Calculated parameters of imidazole derivatives **1–4** in the ground and excited states

Characteristics	dpi (1)	ddi (2)	dmpfpi (3)	dmphnpi (4)
S_0 state				
E (kcal/mol)	0.00	0.00	0.00	0.00
μg (D)	3.30	0.95	3.66	4.14
Excited state DFT				
E (kcal/mol)	1.00	1.52	1.26	1.45
μg (D)	8.46	4.02	9.85	10.04
Dihedral angle (°)				
(C25-C24-N4-C5)	−26.68	−27.59	−25.25	−28.23
(C9-C8-C3-N2)	0.0002	0.0021	0.0028	0.0031
(C11-C8-C3-N2)	−180.00	−179.89	−178.31	−178.99
(C9-C8-C3-N4)	179.99	178.29	178.86	178.98
(C11-C8-C3-N4)	-0.0032	−0.0068	−0.0081	−0.0091
Bond length (Å)				
N2-C3	1.3773	1.3885	1.3772	1.3828
C3-N4	1.4061	1.4054	1.4089	1.4091
C8-C3	1.3854	1.3888	1.3828	1.3891
C9-C8	1.4442	1.4481	1.4485	1.4500
C8-C11	1.4428	1.4462	1.4472	1.4482

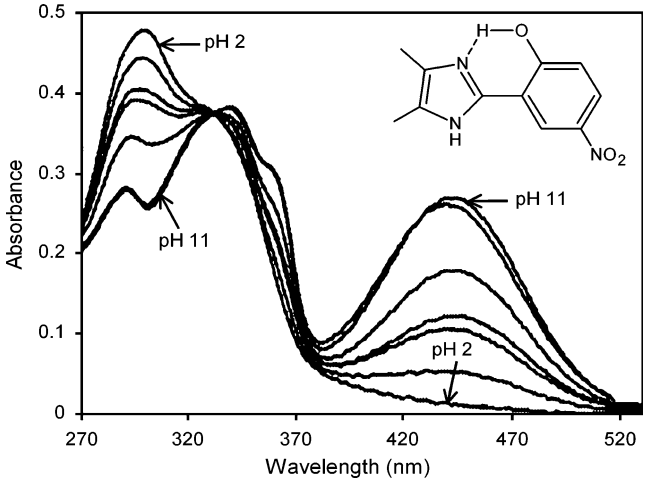

Fig. 3 Absorption spectrum of dmphnpi **4** at different apparent pH solutions

and the refractive indexes of the corresponding solution for the samples and the standard, respectively.

The quantum yield has a tendency to shift to higher with increasing the maximum emission peak wavelength and the observed features of dpi **1** in the solution are determined by specific interactions of the NH hydrogen.

It is evident that the main decay route of the excited state in these compounds and their fluorescence and non-radioactive decay with minor contribution on from the photochemical decay route.

$$k_r = \Phi_p/.\tau \tag{6}$$

$$k_{nr} = 1/\tau - \Phi_p/\tau \tag{7}$$

$$\tau = (k_r + k_{nr})^{-1} \tag{8}$$

Where k_r, k_{nr} are the radiative and non-radiative deactivation, τ_f is the life time of the S_1 excited state.

From the view point of the relationship between maximum emission peak wavelength of fluorescent spectra and decay rate constants, two trends are evident for the imidazole derivatives **1**–**3**. The radiative rate constants (k_r) increases as the maximum emission peak shift to red and the non-radiative decay rate constant (k_{nr}) decreases as the maximum emission peak shift to red.

Imidazole derivatives **1**–**3** as fluorescent chemisensors

The observed non-radiation emission may be due to n-π* transition [23]. Imidazole derivatives have been used to construct highly sensitive fluorescent chemisensors for sensing and imaging of metal ions and its chelates in particular those with Ir^{3+} are major components for organic light emitting diodes [2, 3] and are promising candidates for fluorescent chemisensor for metal ions, if their radiationless channel could be blocked by metal binding. In the presence of transition metal ions such as Hg^{2+}, Pb^{2+} and $Cu^{2+,}$ an enhancement of fluorescence was observed to a different

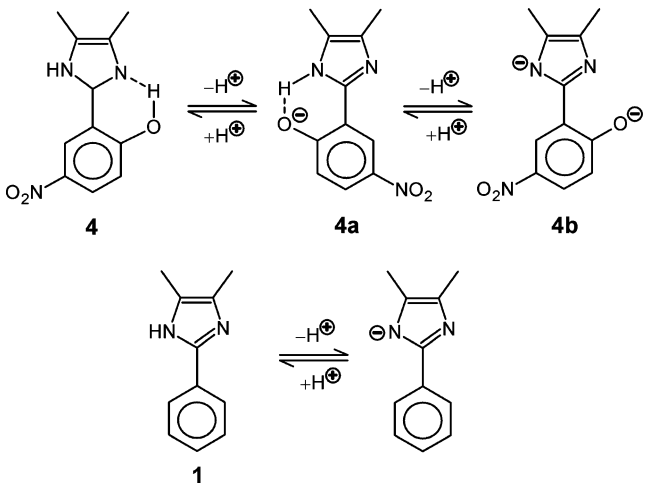

Scheme. 1 The possible deprotonating equilibrium of dpi **1** and dmphnpi **4**

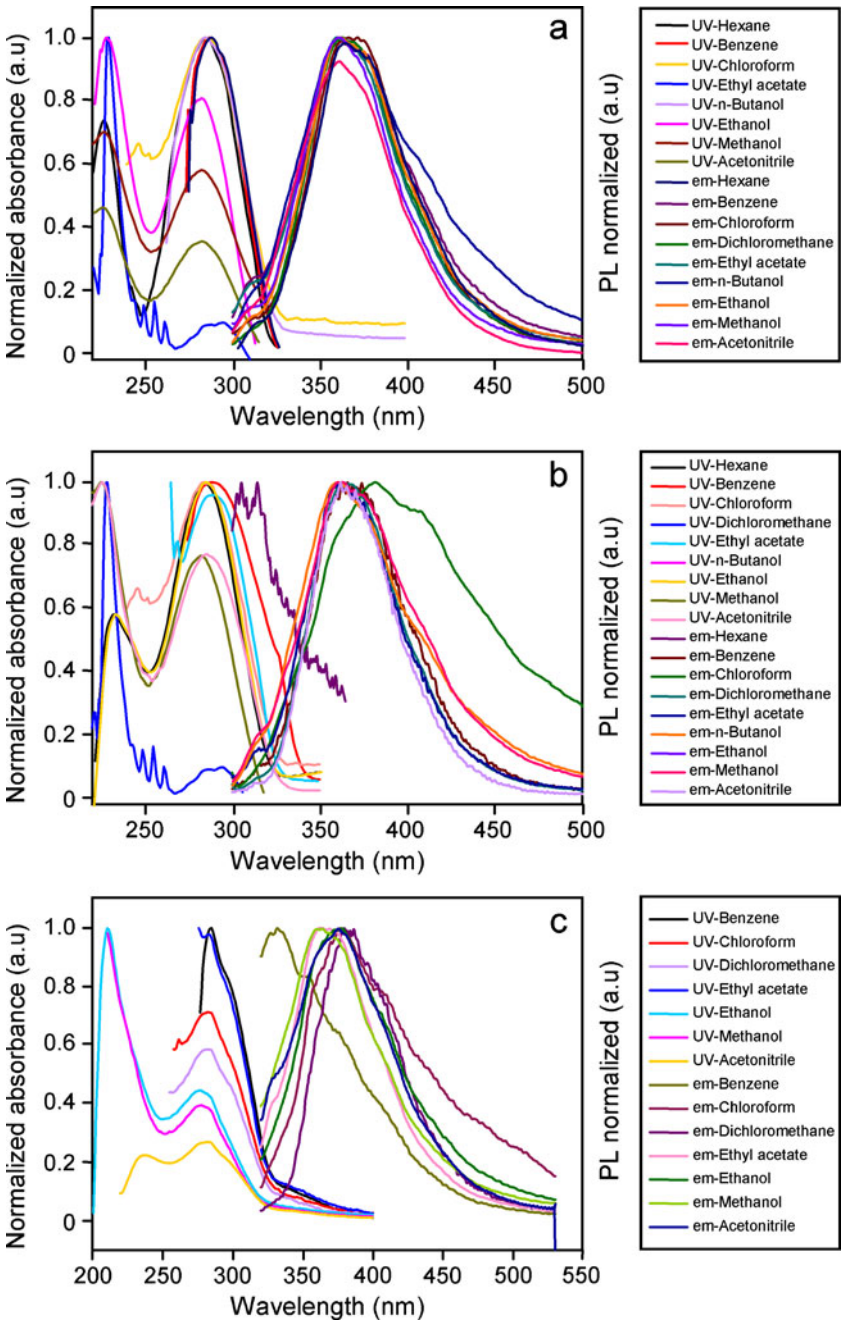

Fig. 4 Absorption and emission spectra of **1**–**4** at different solvents

extent (Table 4) which shows that the metal ions binding, blocks the radiationless decay channel in **1**–**3** (Fig. 6). The radiative (k_r) and non-radiative(k_{nr}) rate constants were calculated for ddi **2** in Cu^{2+} in ACN. It was found that the substantial increase in the quantum yield in the presence of Cu^{2+} is due to dramatic decrease in nonradiative transition whereas the radiation constant remains unchanged within the experimental error. This means that the radiationless decay in ddi **2** is indeed blocked upon metal binding and the emission of chelate (Cu^{2+} ddi) orginates from π-π* state [23].

Halochromisim of imidazole derivative dmphnpi (**4**) in acetonitrile solution

We have measured the absorption spectra of dmphnpi **4** in aprotic solvent acetonitrile at different pH value (Fig. 1a–c) and it was found that the imidazole compound **4** show

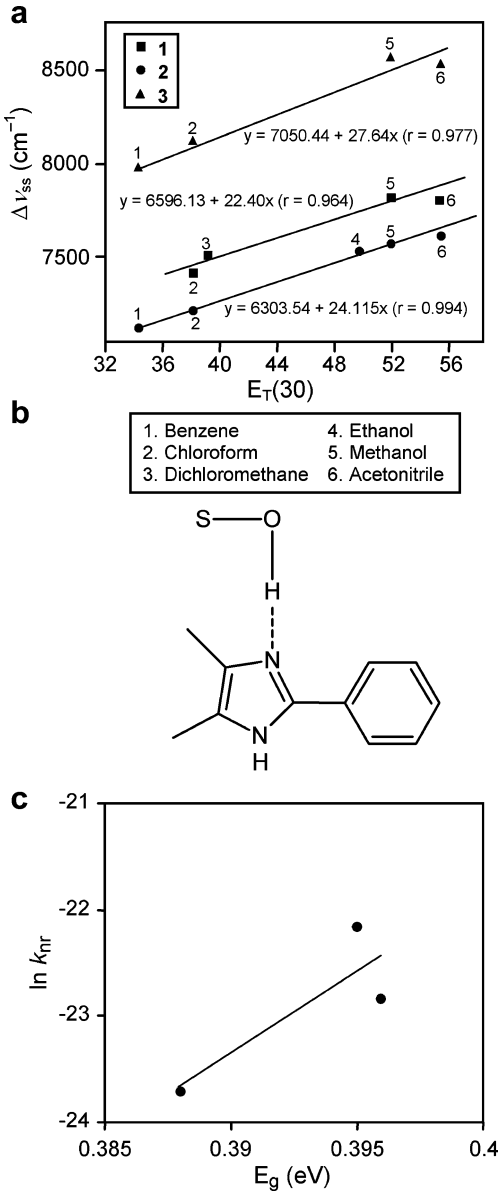

Fig. 5 (**a**) Plot of Stokes shifts versus $E_T(30)$ parameters. (**b**) Stabilization of solvated isomers of **1**–**3**. (**c**) Plot of ln k_{nr} versus the energy gap

halochromic behaviour dependent on the pH. The absorption band was red shifted with increasing pH and the absorption peak (λ_{max}) was located at 286 and 450 nm i.e., as the pH of the solution increases, the absorption bands disappeared and new absorption bands appeared at 286 and 450 nm. There are two isobestic points observed approximately at 325 and 372 nm which may be due to the two deprotonation steps shown in Scheme 1. The first deprotonation step around pH 3.9 is attributed to the loss of phenolic proton forming $[4\text{-H}]^-$ and the second deprotonation step occurs at pH 9.3 is attributed to the formation of doubly deprotonated system $[4\text{-2H}]^{2-}$ (Scheme **1**). Comparison of dmphnpi **4** with a system dpi **1** that lacks the phenolic proton, one can clearly see that the first deprotonation step of dpi **1** is almost identical to the second deprotonation step of dmphnpi **4**, supporting our assumption that the deprotonation step at basic pH of the imidazole ring.

Table 4 Absorption and Fluorescence spectral data of Hg^{2+}, Cu^{2+}, and Pb^{2+} chelates in acetonitrile

Compound	Chemisensor	λ_{em} (nm)	λ_{abs} (nm)
dpi (**1**)	1	226/287.5	383
	$1+Cu^{2+}$	226/289.0	395
	$1+Hg^{2+}$	227/288.0	393
	$1+Pb^{2+}$	226/289.0	384
ddi (**2**)	2	226/286.0	363
	$2+Cu^{2+}$	228/288.0	373
	$2+Hg^{2+}$	228/289.0	378
	$2+Pb^{2+}$	281.0	366
dmpfpi(**3**)	3	239/282.1	375
	$3+Cu^{2+}$	238/282.0	390
	$3+Hg^{2+}$	238/283.0	391
	$3+Pb^{2+}$	239/283.0	390

Intramolecular hydrogen bonding (C-H….O) in dmphnpi (**4**)

Generally a hydrogen bond is formed when the hydrogen atom of a covalent bond of a proton donor molecule interacts with a lone pair electron of an atom of a proton acceptor. Recently, it has been established that a C-H group can be a hydrogen bond donor and although the C-H….O interactions are considered as weak, they form 20–25% of the total number of hydrogen bonds constituting the second

Table 3 Quantum yield and emission kinetics of imidazole derivatives **1**–**4**

Compound	$\lambda_{max\ (nm)}$	ϕ_f	τ_f (ns)	k_r (ns^{-1})	k_{nr} (ns^{-1})	HOMO (a.u)	LUMO (a.u)	Eg (a.u)
dpi (**1**)	383.2	0.92	1.70	0.54	0.05	−0.2784	0.1101	0.388
ddi (**2**)	363.0	0.65	1.44	0.45	0.24	−0.2794	0.1157	0.395
dmpfpi (**3**)	375.6	0.80	1.61	0.50	0.12	−0.2860	0.1110	0.396
dmphnpi (**4**)	–	–	–	–	–	−0.2705	0.1101	0.381

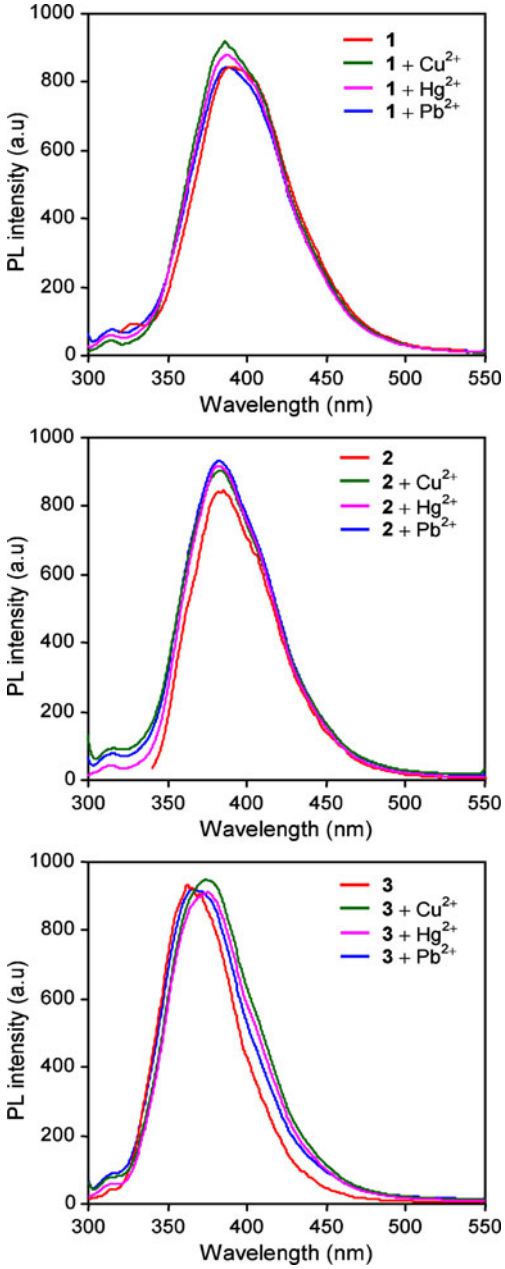

Fig. 6 Fluorescence chemisensors blocking by metal ion binding

most important group [24]. These interactions have been shown to be of greater importance in biological systems in order to elucidate the structure-activity relationship [25]. The C-H…O interaction have been identified from DFT calculation, in which the C-H donor group is strengthened, shortened and blue shifted in the stretching vibrational wave number [26]. The intramolecular H….O distances of H16-O23 and H31-O23 is found to be 2.25° Å and 2.252 Å respectively. The intramolecular C-H….O distance of C3-H24…O23 is found to be 2.53 (1). These distances are significantly shorter than that of the van der Waals separation between the O atom and the H-atom (2.72 Å) [27] indicating the existence of the C-H….O interaction in 4. The calculated C-H….O angle nearly equal to 103.6° is within the angle limit, as the interaction path is not necessarily be linear as several C-H….O hydrogen bonding have a bend structure.

Potential Energy Surface (PES) scan for conformation of hydroxy group in dmphnpi (**4**)

The potential energy surface scan about C25-C27-O34-H35 is performed for O-H bond using B3LYP/6-31G(d,p) level of theoretical approximation for dmphnpi **4.** The torsional angle of C25-C27-O34-H35 for dmphnpi **4** is also relevant coordinate for conformation flexibility within the molecule. During the calculation all the geometrical parameters were simultaneously relaxed while the C25-C27-O34-H35 torsional angles were varied in steps of 0°, 10°, 20°, 30°……..360°. The potential energy surface diagram clearly reveals that the minimum energy conformation corresponds to the one in which –OH group is oriented towards nitrogen atom N4 and is formed by the rotation of 0° or 360° (Fig. 7).

Second Harmonic Generation (SHG) studies of imidazole derivatives **1**–**4**

Second harmonic signal of 2 mV, 1.6 mV and 1.7 mV were obtained for imidazole derivatives **1**–**4** by an input energy

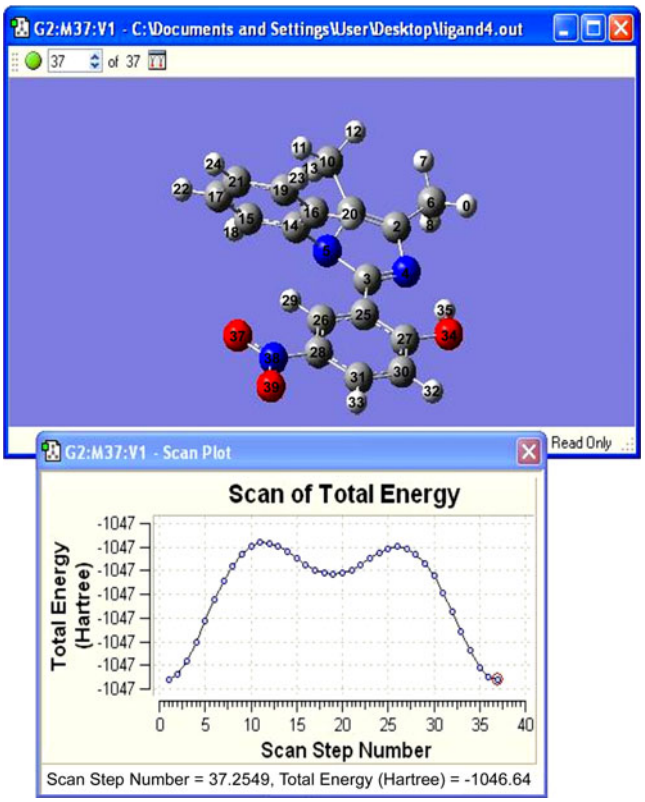

Fig. 7 Energy-minimized molecular modeling structures of dmphnpi **4**

of 4.1 mJ/pulse. But the standard KDP crystal gave a SHG signal of 110 mV/pulse for the same input energy. The second order nonlinear efficiency will vary with the particle size of the powder sample [28]. Higher efficiencies are expected to be achieved by optimizing the phase matching [29]. On a molecular scale, the extent of charge transfer (CT) across the NLO chromophore determines the level of SHG output, the greater the CT, the larger the SHG output.

Hyperpolarizability of imidazole derivatives **1**–**4** by DFT method

In addition to well known empirical rules to estimate qualitatively the microscopic nonlinear response in imidazole derivatives **1–4**, DFT calculation is a more accurate prediction of the NLO activity [30, 31]. The value of second order optical susceptibility in a given NLO system depends on the molecular hyperpolarizability (β), the number of chromophores and the degree of noncentrosymmetry. From Table 5, it was suggested that these compounds **1−3** are polar having non-zero dipole moment, hyperpolarizabilities and hence have well microscopic NLO behaviour [32–34].

Table 5 Electric dipole moment (D), Polarizability (α) and Hyperpolarizability (β_{total}) of **1–4**

Parameter	dpi (**1**)	ddi (**2**)	dmpfpi (**3**)	dmphnpi (**4**)
Electric dipole moment (D)				
μ_x	0.4131	0.0487	−2.0219	−1.7984
μ_y	−3.2726	0.9081	−3.0449	3.7337
μ_z	−0.0078	−0.2707	2.0005	−0.0011
μ_{total}	3.2985	0.9489	3.6551	4.1442
Polarizability (α)				
α_{xx}	168.02	184.04	173.57	177.81
α_{xy}	−0.760	−2.432	−0.589	−3.07
α_{yy}	0.002	131.160	−0.232	131.833
α_{xz}	0.062	1.218	−0.005	0.001
α_{yz}	119.264	−0.044	−4.063	0.002
α_{zz}	43.391	62.236	57.992	55.637
α x 10^{-24} (esu)	70.47	18.68	56.43	18.05
Hyperpolarizability (β_{total})				
β_{xxx}	−594.199	282.650	−346.888	−709.208
β_{xxy}	−8.630	45.587	−10.494	−45.492
β_{xyy}	51.470	48.298	34.811	18.718
β_{yyy}	−38.296	−4.642	−30.3511	−15.776
β_{xxz}	−0.002	−155.959	2.009	−4.738
β_{xyz}	0.212	53.604	20.806	−0.228
β_{yyz}	−0.002.	−16.659	−5.084	−0.256
β_{xzz}	−13.619	26.143	8.328	13.414
β_{yzz}	−8.630	−37.297	−5.084	3.773
β_{zzz}	−0.004	13.261	0.254	0.454
β x 10^{-31} (esu)	48.26	34.62	50.01	58.72

UV-visible spectroscopy Vs NLO activity in imidazole derivatives **1**–**4**

It can be very helpful in the investigation of NLO materials making it possible to check, apart from NLO responses, also spectroscopic absorbances in the appropriate wavelength. Thus, the wavelengths obtained by UV-visible spectral analysis can be helpful in planning the synthesis of the promising NLO materials only [34]. The solution electronic absorption spectral studies of compound designed to possess NLO properties are important for two specific reasons. First, it is necessary to know the transparency region. Second, the solvatochromic behaviour of the sample is generally considered as indicative of high molecular first hyperpolarizability [34–38].

To determine the transference region and hence to know the suitability of these compounds **1–4** for microscopic nonlinear optical applications, the UV-visible spectra have been recorded by using the spectrometer in the range of 190-1,100 nm. Table 1 revealed that these compounds show absorption spectra in the UV region between 210 and 290 nm. The increased transparency in the visible region might enable the microscopic NLO behaviour with non-zero values [28, 39, 40]. All the absorption bands are due to π→π* transitions. The β values (Table 5) computed here might be correlated with UV-visible spectroscopic data in order to understand the molecular-structure and NLO relationship in view of a future optimization of the microscopic NLO properties. Therefore, the validity of B3LYP/6-31G(d,p) approximation used in all the computations here might also be illustrated by analyzing the relationship between calculated β values and measured values of λ_{max} (Table 1). The band at around 280 nm exhibits a solvatochromic shift, characteristic of a large dipole moment (Table 5) and frequently suggestive of a large hyperpolarizability (Tables 5). These compounds show red shift in absorption with increasing solvent polarity, accompanied with the upward shifts non-zero values in the β-components [21]. From β-values it was found that all these imidazole compounds are polar having non-zero dipole moment and such compounds have large hyperpolarizabilities and hence have rather well microscopic NLO behaviour [28, 30, 35, 36].

Natural Bond Orbital (NBO) analysis of imidazole derivatives **1**–**4**

NBO analysis was performed to identify and confirm the possible intra and intermolecular interactions between the units that would form the hydrogen bonding. A useful aspect of the NBO method is that it gives information about interactions in both filled and virtual orbital spaces that could enhance the analysis of intra and intermolecular

Table 6 Significant donor-acceptor interactions of imidazole derivatives **1–4** and their second-order perturbation energies (kcal/mol)

Donor	Acceptor	dpi (**1**)	ddi (**2**)	dmpfpi (**3**)	dmphnpi (**4**)
C8-C11	N2-C3	18.20	17.76	14.39	14.50
C8-C11	C9-C10	18.49	19.40	20.61	18.84
C8-C11	C12-C13	20.51	19.76	20.54	19.65
C12-C13	C8-C11	19.61	20.34	19.80	20.62
C12-C13	C9-C10	19.40	19.06	19.05	18.19
LPN-2	C3-N4	11.44	11.9	11.77	11.36
LPN-4	C1-C5	27.57	8.79	23.62	26.44
LPN-4	N2-C3	38.90	10.94	33.31	36.35
N2-C3	C1-C5	32.33	31.28	30.07	31.60
C9-C10	C8-C11	20.23	–	18.50	19.68
C9-C10	C12-C13	20.89	–	21.62	21.56
C14-C17	C15-C16	–	–	19.21	–
C12-C13	C8-C11	–	–	308.69	–
C8-C11	C9-C10	–	–	–	280.88
C25-C26	C27-C30	–	19.58	–	–
C25-C26	C28-C29	–	20.35	–	–

interactions. The second order Fock matrix was carried out to evaluate the donor–acceptor interactions in the NBO analysis [41]. The interactions result is a loss of occupancy from the localized NBO of the idealized Lewis structure into an empty non-Lewis orbital. For each donor (i) and acceptor (j), the stabilization energy E(2) associated with the delocalization i → j is estimated as

$$E(2) = \Delta E_{ij} = q_i \frac{F(i,j)^2}{\varepsilon j - \varepsilon i} \quad (9)$$

Where q_i is the donor orbital occupancy, εi and εj are diagonal elements and F(i, j) is the off diagonal NBO Fock matrix element. Natural bond orbital analysis provides an efficient method for studying intra and intermolecular bonding and interaction among bonds and also provides a convenient basis for investigating charge transfer or conjugative interaction in molecular systems. Some electron donor orbital, acceptor orbital and the interacting stabilization energy resulted from the second-order microperturbation theory are also reported [42]. The larger the *E*(2) value, the more intensive is the interaction between electron donors and electron acceptors, i.e., the more donating tendency from electron donors to electron acceptors and the greater the extent of electron density transfer (EDT) or hyperconjugative interaction of the whole system. Delocalization of electron density between occupied Lewis-type (bond or lone pair) NBO orbitals and formally unoccupied (antibond or Rydgberg) non-Lewis NBO orbitals correspond to a stabilizing donor–acceptor interaction. NBO analysis have been performed on the molecule at the DFT/B3LYP/6-31G(d,p) level in order to elucidate the intramolecular, rehybridization and delocalization of electron density within the molecule. The intramolecular interaction are formed by the orbital overlap between σ (C-C) and σ* (C-C) bond orbital which results intramolecular charge transfer (ICT) causing stabilization of the system. These interactions are observed as increase in electron density (ED) in C-C antibonding orbital that weakens the respective bonds.

Several donor-acceptor interactions are observed in imidazole derivatives **1–4** and among the strongly occupied NBOs, the most important delocalisation sites are in the π system and in the lone pairs (n) of the nitrogens, oxygen and fluorine of the imidazole derivatives **1–4** . The σ system shows some contribution to the delocalization and almost the donor-acceptor interactions are same in all these compounds and the important contributions to the dilocalization corresponds to the donor-acceptor interactions are LPN4 → N2 – C3, LPN4 → C1-C5, N2-C3 → C1-C5, C12-C13 → C8-C11 (3) , LPN4 → C9-C10 and C8-C16 →

Table 7 Percentage of p-character on each natural atomic hybrid of the Natural Bond Orbital (NBO) of imidazole derivatives **1–4**

NBO	Atom	dpi (**1**)	ddi (**2**)	dmpfpi (**3**)	dmphnpi (**4**)
C_1-N_2	C_1	73.05	73.10	73.16	73.04
	N_2	71.31	70.01	71.35	71.33
C_1-C_5	C_1	99.92	99.90	99.92	62.23
	C_5	99.93	98.87	99.92	60.78
N_2-C_3	N_2	99.72	99.81	99.68	99.71
	C_3	99.92	99.78	99.89	99.88
N_2-C_3	N_2 C_3	–	–	–	–
C_8-C_{11}	C_8	99.97	99.96	99.95	99.97
	C_{11}	99.97	99.95	99.95	99.96
C_8-C_{11}	C_8 C_{11}	–	–	–	–
C_8-C_{11}	C_8 C_{11}	–	–	–	–
C_9-C_{10}	C_9	99.96	99.95	99.95	99.96
	C_{10}	99.96	99.96	99.96	99.96
C_9-C_{10}	C_9 C_{10}	–	–	–	–
C_{12}-C_{13}	C_{12}	99.96	99.96	99.95	99.96
	C_{13}	99.96	99.96	99.95	99.96
C_{12}-C_{13}	C_{12} C_{13}	–	–	–	–
$4N_2$	N_2	65.24	68.30	65.46	65.32
$4N_4$	N_4	99.91	77.45	96.78	98.30
N_2-C_3	N_2	99.72	99.81	99.68	99.71
	C_3	99.92	99.78	99.68	99.88
20F	–	–	–	99.95	–
LPO 14	–	–	–	–	97.81

C9-C10 (4) (Table 6). NBO analysis clearly manifests the evidence of the intramolecular hydrogen bonding by charge transfer from LpN4 to antibonding orbital of C9-C10 shows that the hydroxy group is inclined towards the nitrogen atom N4 side (**2** and **3**).

The percentage of p-character [43] in each NBO natural atomic hybrid orbital is presented in Table 7. The C1-N2 bond of imidazole ring has a p-character around 70–73%. However, for all other carbon hybrids in benzene ring, almost 100% p-character was observed. Finally, the σ lone pair on nitrogen has very strong deviation to around 65% in all the compounds whereas in the case of N2-C3 bond, the % of p-character on N2 and C3 atoms are strongly increased to around 99% but the σ lone pair on nitrogen atom N4 has a increase to about 96.8–99.9% in all the compounds except compound **2** where the p-character is reduced to 77.51%. The charge distribution shows that the more negative charge is concentrated on nitrogens, fluorine and oxygen whereas the partial positive charge resides at hydrogens. The charge distributions of **1–4** calculated by the NBO and Mulliken methods and the charges are displayed in Table 8. The two methods predict the same tendencies i.e., compared to nitrogen atom N4, N2 nitrogen atom is acidic in all the imidazole derivatives i.e., the hydrogen atom bonded to N2 is easily replaceable (**1**) and the nitrogen atom N4 is basic site [44]. From the Table 2, one can see that the excited molecule leads to increase in the electron density at N2 nitrogen atom and then the excited molecule emits luminescence and turns to the ground state.

HOMO-LUMO energies of imidazole derivatives **1-3** by DFT method

Molecular orbital and their properties, like energy are very useful for physicists and chemists and their frontier electron density used for predicting the most reactive position in π-electron systems and also explained several types of reaction in conjugated system [45]. Moreover, eigen values of LUMO and HOMO and their energy gap reflect the

Table 8 The charge distribution calculated by Mulliken and natural bond orbital (NBO) methods for imidazole derivatives **1–4**

Atom	dpi (**1**)		ddi (**2**)		dmpfpi (**3**)		dmphnpi (**4**)	
	NBO	Mulliken	NBO	Mulliken	NBO	Mulliken	NBO	Mulliken
1C	0.1869	0.1869	0.2005	0.2005	0.1766	0.1766	0.1826	0.1825
2N	−0.5361	−0.5361	−0.5571	−0.5571	−0.5218	−0.5218	−0.5252	−0.5252
3C	0.4546	0.4546	0.4167	0.4167	0.4106	0.4106	0.4270	0.4270
4N	−0.6531	−0.3872	−0.7100	−0.7100	−0.6186	−0.6186	−0.6203	−0.3420
5C	0.2922	0.2922	0.1393	0.1393	0.2767	0.2767	0.2828	0.2828
6C	−0.3732	−0.0116	−0.4581	0.0075	−0.3784	−0.083	0.3756	−0.0156
7C	−0.3835	−0.0298	−0.4565	0.0754	−0.3852	−0.0247	−0.3837	−0.0330
8C	0.1022	−0.1022	−0.0264	−0.0264	0.0696	0.0696	0.0798	0.0798
9C	−0.1111	0.0041	−0.1631	−0.0846	−0.0963	0.0227	−0.1166	−0.0008
10C	−0.0898	−0.0024	−0.2162	−0.0136	−0.1344	−0.0270	−0.0893	−0.0024
11C	−1.2227	−0.0647	−0.1749	−0.0563	−0.1025	0.0048	0.2302	0.2302
12C	−0.0925	−0.0091	−0.2169	−0.0160	−0.1368	−0.0308	−0.0943	−0.0044
13C	−0.0825	0.00	−0.1849	−0.0161	0.3313	0.3314	−0.0886	−0.0019
25C	–	–	−0.2045	0.0058	–	–	–	–
26C	–	–	−0.1489	0.0884	–	–	–	–
27C	–	–	0.1085	0.1085	–	–	–	–
28C	–	–	−0.1937	0.0115	–	–	–	–
29C	–	–	−0.2032	0.0029	–	–	–	–
30C	–	–	−0.1773	0.0420	–	–	–	–
14C	–	–	–	–	0.2160	0.2160	–	–
15C	–	–	–	–	−0.0760	0.0336	–	–
16C	–	–	–	–	−0.0973	0.0014	−0.6080	−0.2770
17C	–	–	–	–	−0.0947	0.0041	–	–
18C	–	–	–	–	−0.0948	0.0008	–	–
19C	–	–	–	–	−0.0791	0.0127	–	–
20F	–	–	–	–	−0.0791	−0.3299	–	–

chemical activity of the molecule. Recently the energy gap between highest occupied molecular orbital (HOMO) and the lowest unoccupied molecular orbital (LUMO) have been used to prove the bioactivity from intramolecular charge transfer (ICT) [46, 47]. The HOMO-LUMO energy gap for **1**–**3** were calculated by B3LYP/6-31G(d,p) and the HOMO-LUMO orbital picture of dpi **1** is given in Fig. 8. From the HOMO-LUMO orbital picture it was found that the filled π orbital (HOMO) is mostly located on the aldehydic phenyl ring of the imidazole derivative and the unfilled π* orbital (LUMO) on the imidazole ring with aniline phenyl ring. Therefore introduction of an electron-donating substituent into the aniline phenyl ring raises the energy of the LUMO resulting in a blue-shift of the emission. On the otherhand, the introduction of the electron-donating substituent into the aldehydic phenyl ring raises the energy of the HOMO, leading to the red shift of the emission [48, 49].

The energy gap (E_g) of all the reported compounds **1**−**4** were calculated from the HOMO and LUMO levels. The plot of ln(k_{nr}) versus the energy gap for compounds **1**–**3** (Fig. 5c) shows linear relationship.The decrease in the HOMO and LUMO energy gap explains the probable charge transfer (CD) taking place inside the chromophore. The energy gap law predicts that the rate of non-radiative decay increases when the energy gap separating the ground and excited state decreases. This relation is based on the vibrational overlap between the ground state and excited state and k_{nr} is a function of Frank-Condon overlap integral. In the cases of compounds having similar excited states and vibratonal coupling, a simplified form of the energy gap law is obtained that predicts a linear relationship between ln (k_{nr}) and the energy gap. This correlation suggests that decay rate constants are due to the energy gap of the compounds [50] and from the emission spectra it is observed that the emission of **1**–**3** is due to π-π* transition. A good correlation was found between the computed and experimental wave numbers (Fig. 9, Table 9) and calculated wave numbers obtained by DFT/B3LYP/6-31G(d,p) method [51, 52]. Experimental C=N and C-N stretching wave-numbers have been lowered due to conjugation and π-electron delocalization.

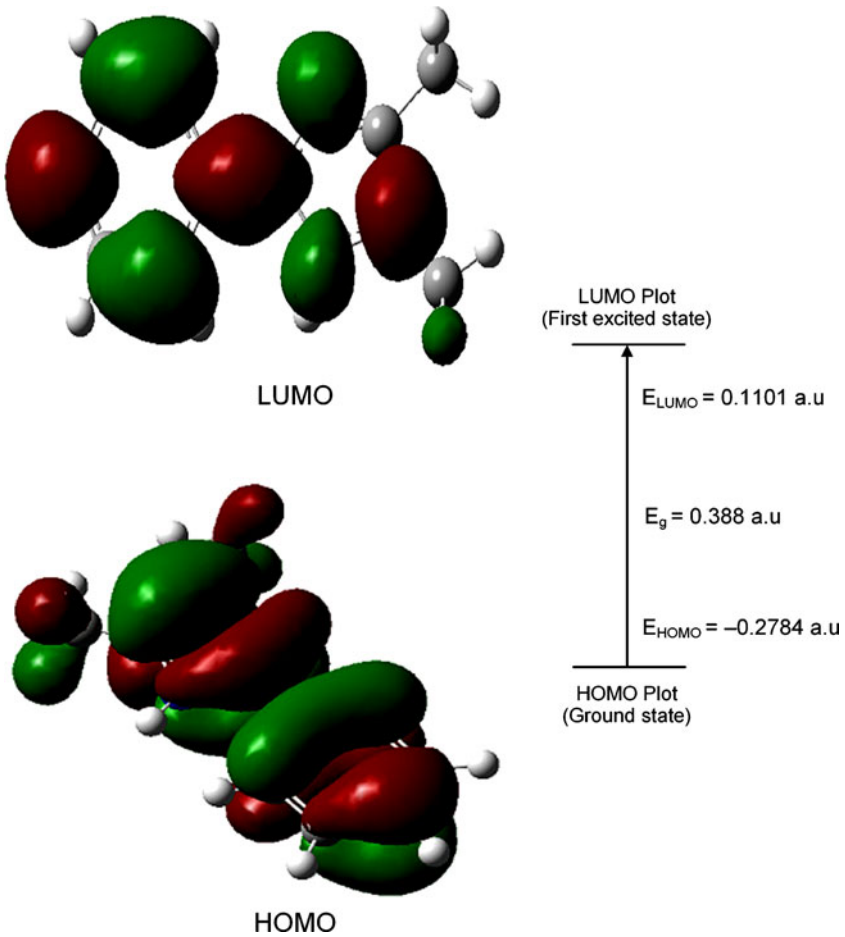

Fig. 8 HOMO-LUMO orbital picture of dpi **1**

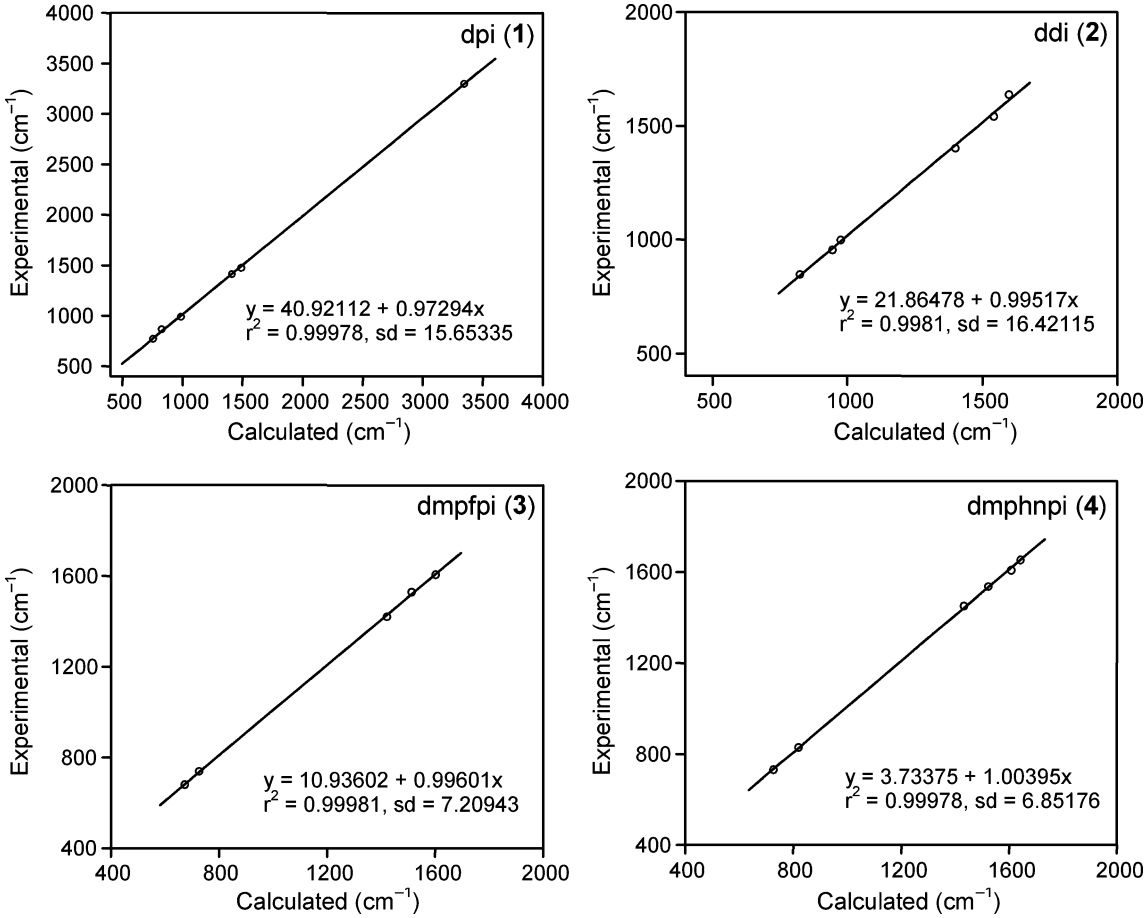

Fig. 9 Graphical correlation between experimental and theoretical absorption frequencies of **1–4**

Conclusion

We have developed Imidazole derivative as a new set of fluorescent chemisensors for transition metal ions Hg^{2+}, Pb^{2+} and Cu^{2+}. Especially the imidazole derivative ddi (**2**) shows a highly sensitive and selective response in its emission towards Cu^{2+} ion. We suggest that ddi (**2**) operates under the mechanism that metal binding block the radiationless n-π* transition in ddi (**2**)**.** Further work we focused that the increased transparency of these imidazole derivatives in the visible region might enable the microscopic NLO behaviour with non-zero values and all the

Table 9 Experimental and theoretical IR spectral data (cm^{-1}) of imidazole derivatives **1–4**

dpi (**1**)		ddi (**2**)		dmpfpi (**3**)		dmphnpi (**4**)		Assignment
Experimental (υ, cm^{-1})	Theoretical (υ, cm^{-1})	Experimental (υ, cm^{-1})	Theoretical (υ, cm^{-1})	Experimental (υ, cm^{-1})	Theoretical (υ, cm^{-1})	Experimental (υ, cm^{-1})	Theoretical (υ, cm^{-1})	
1604	1636	1599	1637	1603	1605	1608	1608	$\nu_{C=N}$
987	991	975	998	1030	1049	1103	1105	ν_{C-N}
3345	3682	–	–	–	–	–	–	ν_{N-H}
–	–	–	–	–	–	1642	1653	ν_{N-OH}
1412,1489	1415,1474	1400,1542	1402,1541	1422,1514	1420,1528	1434,1523	1451,1536	$\nu_{C=C}$
755,827	772,870, 1511,1463	944,823	955,846	727,674	738,690	820,727	829,738	ν_{C-H}, ν_{CH3}

absorption bands are due to π-π* transition. Potential energy surface (PES) scan about C25-C27-O34-H35 is performed for –OH bond using B3LYP/6-31G(d,p) level for dmphnpi (**4**) which reveals that the minimum energy conformation corresponds to the one in which the –OH group is oriented towards the N4 nitrogen atom. The photophysical studies were carried out, NBO and HOMO-LUMO analysis were carried out theoretically and analysed in detail.

Acknowledgements One of the author Dr. J. Jayabharathi, Reader in Chemistry, Annamalai University is thankful to Department of Science and Technology [No. SR/S1/IC-07/2007], University Grants commission (F. No. 36-21/2008 (SR)) for providing fund to this research work.

References

1. Santos J, Mintz EA, Zehnder O, Bosshard C, Bu XR, Gunter P (2001) New class of imidazoles incorporated with thiophenvinyl conjugation pathway for robust nonlinear optical chromophores. Tetrahedron Lett 42:805–808
2. Huang WS, Lin JT, Chien CH, Tao YT, Sun SS, Wen YS (2004) Highly phosphorescent Bis-cyclometalated Iridium complexes containing Benzimidazole-Based ligands. Chem Mater 16:2480–2488
3. Chen CH, Shi J (1998) Metal chelates as emitting materials for organic electroluminescence. Coord Chem Rev 171:161–174
4. Kamidate T, Yamaguchi K, Segawa T (1989) Lophine Chemiluminescence for Determination of Chromium(VI) by Continuous Flow Method H. Watanabe. Anal Sci 5:429–433
5. Nakashima K, Yamasaki H, Kuroda N, Akiyama S (1995a) Evaluation of lophine derivatives as chemiluminogens by a flow injection method. Anal Chim Acta 303:103–107
6. Nakashima K (2003b) Lophine derivatives as versatile analytical tools. Biomed Chromatogr 17:83–95
7. MacDonald A, Chain KW, Nieman TA (1979) Lophine chemluminescence for metal ion determinations. Anal Chem 51:2077–2082
8. Marino DF, Ingle JD Jr (1981) Determination of Chromium(VI) in water by lophine chemiluminescence. Anal Chem 53:294–298
9. Lipshutz BH (1986) Five-membered hetero aromatic rings as intermediates in organic synthesis. Chem Rev 86:795–819
10. Ucucu U, Karaburun NG, Isikdag I (2001) Synthesis and analgesic activity of some 1-benzyl-2-substituted-4, 5-diphenyl-1H-imidazole derivatives. I L Farmaco 56:285–290
11. Nakashima K, Taguchi Y, Kuroda N, Akiyama S, Duan G (1993) 2-(4-Hydrazinocarbonylphenyl)-4, 5-diphenylimidazole as a versatile fluorescent derivatization reagent for the high-performance liquid chromatographic analysis of free fatty acids. J Chromatogr 619:1–8
12. Yagi K, Soong CF, Irie M (2001) Synthesis of fluorescentdiarylethenes having a 2, 4, 5-triphenylimidazole chromophore. J Org Chem 66:5419–5423
13. Gostev FE, Kol'tsova LS, Petrukhin AN, Titov AA, Shiyonok AI, Zaichenko NL, Marevtsev VS, Sarkisov M (2003) Spectral luminescence properties and dynamics of intramolecular processes in 2,4,5-triarylimidazoles. J Photochem Photobiol A 156:15–22
14. Feng K, Hsu F-L, Veer DVD, Bota K, Bu XR (2004) Tuning fluorescence properties of imidazole derivatives with thiophene and thiozole. J Photochem Photobiol A 165:223–228
15. Hennessy J, Testa AC (1972) Photochemistry of phenylimidazoles. J Phys Chem 76:3362–3365
16. Guassian 03 program, (Gaussian Inc., Wallingford CT) 2004
17. Schlegel HB (1982) Optimization of equilibrium geometries and transition structures. J Comput Chem 3:214–218
18. Jayabharathi J, Thanikachalam V, Saravanan K (2009) Effect of substituents on the photoluminescence performance of Ir(III) complexes: Synthesis, electrochemistry and photophysical properties. J Photochem Photobiol A 208:13–20
19. Ren P, Liu T, Qin J, Chen C (2003) A new approach to suppress nonlinearity-transparency trade-off through coordination chemistry: syntheses and spectroscopic study on second-order nonlinear optical properties of a series of square-pyramidal zinc(II) complexes. Spectrochim Acta A 59:1095–1101
20. Fridmam N, Kaftory M, Speiser S (2007) Structures and photophysics of lophine and double lophine derivatives. Sens Actuators B 126:107–115
21. Balamurali MM, Dogra SK (2004) Intra- and Intermolecular proton transfer in methyl-2-hydroxynicotinate. J Luminescence 110:147–163
22. Mazumdar S, Manoharan R, Dogra SK (1989) Solvatochromic effects in the fluorescence of a few diamino aromatic compounds. J Photochem Photobiol A 46:301–314
23. Zhou Z, Fahrni CJ (2004) A fluorogenic probe for the copper(I)-catalyzed azide-alkyne ligation reaction: modulation of the fluorescence emission via $^{3}(n,\pi^*)$-$^{1}(\pi, \pi^*)$ inversion. J Am Chem Soc 126:8862–8863
24. Weiss MS, Brandl M, Suhnel J, Pal D, Hilgenfeld R (2001) More hydrogen bonds for the (structural) biologist. Trends Biochem Sci 26:521–523
25. Riebeiro-Claro PJA, Drew MGB, Felix V (2002) C-H….O bonded dimers in 2-methoxy-benzaldehyde studied by X-ray crystallography, Vibrational spectroscopy, and ab initio calculations. Chem Phys Lett 356:318–324
26. Hermansson K (2002) Blue-shifting Hydrogen bonds. J Phys Chem A 106:4695–4702
27. Sato H, Dybal J, Murakami R, Noda I, Ozaki Y (2005) Infrared and Raman spectroscopy and quantum chemistry calculation studies of C-H….O hydrogen bondings and thermal behaviour of biodegradable polyhydroxyalkanoate. J Mol Struct 744–747:35–46
28. Porter Y, OK KM, Bhuvanesh NSP, Halasyamani PS (2001) Synthesis and Characterization of Te_2SeO_7: A Powder Second-Harmonic-Generating Study of TeO_2, Te_2SeO_7, Te_2O_5, and $TeSeO_4$. Chem Mater 13:1910–1915
29. Narayana Bhat M, Dharmaprakash SM (2002) Growth of nonlinear optical γ-glycine crystals. J Cryst Growth 236:376–380
30. Karakas A, Elmali A, Unver H, Svoboda I (2004) Nonlinear optical properties of some derivatives of salicylaldimine-based ligands. J Mol Struct 702:103–110
31. Unver H, Karakas A, Elmali A (2004) Nonlinear optical properties, spectroscopic studies and structure of 2-hydroxy-3-methoxy-N-(2-chloro-benzyl)-benzaldehyde-imine. J Mol Struct 702:49–54
32. Lee IS, Shin DM, Yoon Y, Shin SM, Chung YK (2003) Synthesis and non-linear optical properties of (alkyne)dicobalt octacarbonyl complexes and their substitution derivatives. Inorg Chim Acta 343:41–50
33. Mang C, Wu K, Zhang M, Hong T, Wei Y (2004) First-priciple study on second-order optical nonlinearity of some ferrocenyl complexes. J Mol Struct (Theochem) 674:77–82
34. Justin Thomas KR, Lin JT, Wen YS (1999) Synthesis, spectroscopy and structure of new push-pull ferrrocene complexes containing heteroaromatic rings (thiophene and furan) in the conjugation chain. J Organomet Chem 575:301–309
35. Albert IDL, Marks TJ, Ratner MA (1998) Large molecular hyperpolarizabilities in "push-pull" porphyrins. Molecular planarity and auxiliary donor-acceptor effects. Chem Mater 10:753–762

36. Zhou Y, Feng S, Xie Z (2003) Investigation nonlinear optical property of novel *para*-phenylenealkyne macrocycles. Opt Mater 24:667–670
37. Dworczak R, Fabian WMF, Reidlinger C, Rumpler A, Schachner J, Zangger K (2002) Nonlinear optical properties of diazabutadienes and hexatrienes; experimental and computational aspects. Spectrochim Acta A 58:2135–2144
38. Di Bella S, Fragala I, Ledoux I, Diaz-Garcia MA, Lacroix PG, Marks TJ (1994) Sizable second-order nonlinear optical response of donor-acceptor bis(salicylaldiminato)nickel(II) schiff base complexes. Chem Mater 6:881–883
39. Prabhu SG, Rao PM, Bhat SI, Upadyaya V, Inamdar SR (2001) Growth and characterization of N-(2-Chlorophenyl)-(1-Propanamide)-a nonlinear organic crystal. J Cryst Growth 233:375–379
40. Crasta V, Ravindrachary V, Bharantri RF, Gonsalves R (2004) Growth and characterization of an organic NLO crystal: 1-(4-methylphenyl)-3-(4-methoxyphenyl)-2-propen-1-one. J Crystal Growth 267:129–133
41. Szafran M, Komasa A, Adamska EB (2007) Crystal and molecular structure of 4-carboxypiperidinium chloride (4-piperidinecarboxylic acid hydrochloride). J Mol Struct 827:101–107
42. Jun-na L, Zhi-rang C, Shen-fang Y (2005) Study on the prediction of visible absorption maxima of azobenzene compounds. J Zhejiang Univ Sci 6B:584–590
43. Reed AE, Curtiss LA, Weinhold F (1988) Intermolecular interactions from a natural bond orbital, donor-acceptor viewpoint. Chem Rev 88:899–926
44. Wang G, Lian F, Xie Z, Su G, Wang L, Jing X, Wang F (2002) Novel bis(8-hydroxyquinoline)phenolato–aluminum complexes for organic light-emitting diodes. Synth Met 131:1–5
45. Fukui K, Yonezawa T, Shingu H (1952) A molecular orbital theory of reactivity in aromatic hydrocarbons. J Chem Phys 20:722–725
46. Padmaja L, Ravikumar C, Sajan D, Hubert Joe I, Jayakumar VS, Pettit GR, Faurskov Neilsen O (2009) Density functional study on the structural conformations and intramolecular charge transfer from the vibrational spectra of the anticancer drug combretastatin-A2. J Raman Spectrosc 40:419–428
47. Ravikumar C, Hubert Joe I, Jayakumar VS (2008) Charge transfer interactions and nonlinear optical properties of push-pull chromophore benzaldehyde phenylhydrazone: a vibrational approach. Chem Phys Lett 460:552–558
48. Sun Q, Li Z, Zeng X, Ge M, Wang D (2005) Structures and properties of the hydrogen-bond complexes: theoretical studies for the coupling modes of the pyrazole-imidazole system. J Mol Struct (Theochem) 724:167–172
49. Chai SY, Zhou R, An ZW, Kimura A, Fukuho K, Matsumura M (2005) 5-Coordinated aluminium complexes having two 2, 4-dimethyl-8-hydroxyquinoline ligands and a phenolic ligand as possible materials for white emission organic light emitting devices. Thin solid films 479:282–287
50. Brooks J, Babayan Y, Lamansky S, Djurovich PI, Tsyba I, Bau R, Thompson ME (2002) Synthesis and characterization of phosphorescent cyclometalated platinum complexes. Inorg Chem 41:3055–3066
51. Silverstein M, Clayton Basseler G, Morill C (1981) Spectrometric identification of organic compounds. Wiley, New york
52. Shanmugam R, Sathyanarayana DN (1984) Raman and polarized infrared spectra of pyridine-2thione. Spectrochim Acta A 40:757–761